

pubs.acs.org/journal/apchd5 Article

# Photoexcited Free Carrier Dynamics in $Bi_2Se_3$ , $(Bi_{0.75}In_{0.25})_2Se_3$ , and $(Bi_{0.50}In_{0.50})_2Se_3$ : From Topological to Band Insulator

Teng Shi,\* Kateryna Kushnir, Zhengtianye Wang, Stephanie Law, and Lyubov V. Titova\*



Cite This: ACS Photonics 2020, 7, 2778–2786



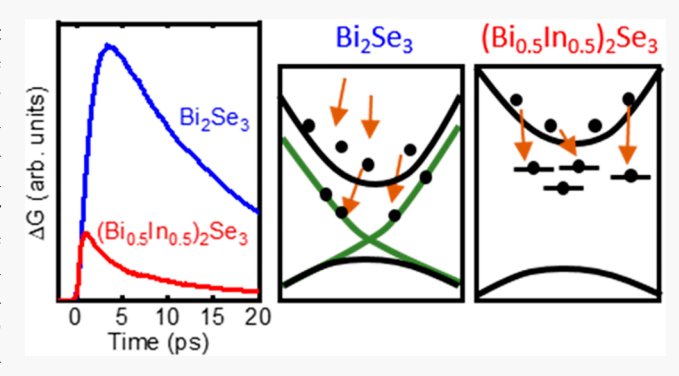
**ACCESS** 

Metrics & More

Article Recommendations

Supporting Information

**ABSTRACT:** Replacing some Bi with In in  $Bi_2Se_3$  transforms it from a topological insulator to a band insulator. Here, we have used time-resolved terahertz spectroscopy to investigate photoexcited carrier dynamics in  $(Bi_{1-x}In_x)_2Se_3$  films with indium concentration x = 0%, 25%, and 50%. In  $Bi_2Se_3$ , optically excited carriers scatter from the bulk conduction band states into high mobility topological surface states within picoseconds after excitation. We demonstrate that a second set of Dirac surface states, located ~1.5–1.8 eV above the conduction band minimum and accessible to carriers excited by 3.1 eV pulses, is characterized by a higher mobility than the surface states within the band gap that dominate equilibrium conductivity. In  $(Bi_{0.75}In_{0.25})_2Se_3$  and  $(Bi_{0.50}In_{0.50})_2Se_3$ , which are insulating without photoexcitation, the



dynamics of photoexcited free carriers are affected by the twin domain boundaries and are sensitive to the disorder introduced by indium substitution. Transient conductivity rise time, as well as the mobility and lifetime of the photoexcited carriers in  $(Bi_{1-x}In_x)_2Se_3$  films, can be tuned by the indium content, enabling tailoring of band insulators that have the desired optoelectronic properties and are fully structurally compatible with the topological insulator  $Bi_2Se_3$  for applications in high-speed photonic devices based on topological insulator/band insulator heterostructures.

**KEYWORDS:** topological insulator, terahertz spectroscopy,  $Bi_2Se_3$ ,  $(Bi_{1-x}In_x)_2Se_3$ , carrier dynamics

opological insulators (TIs) are quantum materials where a full band gap in the bulk coexists with gapless metallic surface states (SS) that are topologically protected by timereversal symmetry and spin-orbit interactions. 1-3 New transport and optical phenomena that emerge in these systems make them attractive for fundamental physics investigations as well as for potential device applications. 4-6 The most widely studied TI is Bi<sub>2</sub>Se<sub>3</sub>, where the bulk band gap is relatively large at ~0.35 eV and topological surface states have been observed experimentally and described theoretically. 2,7-12 When a fraction of Bi atoms are substituted with In to obtain  $(Bi_{1-x}In_x)_2Se_3$ , the system undergoes a series of phase transitions, transforming from a TI at x = 0 to a trivial metallic state at  $3\% \le x \le 7\%$ , and to a true band insulator (BI) at higher In content. Varying In content in (Bi<sub>1-x</sub>In<sub>x</sub>)<sub>2</sub>Se<sub>3</sub> thus enables tuning the band structure and achieving unique electronic and optical properties. Moreover, the resulting alloy retains the rhombohedral  $D_{3d}^5$  crystal structure of  $Bi_2Se_3$  for up to x = 1, and is structurally compatible with  $Bi_2Se_3$ . In fact, the lattice mismatch between Bi<sub>2</sub>Se<sub>3</sub> and In<sub>2</sub>Se<sub>3</sub> is only 3%, and high quality Bi<sub>2</sub>Se<sub>3</sub> TI layers can be grown by molecular beam epitaxy (MBE) on  $(Bi_{1-x}In_x)_2Se_3$  with x up to 75%. This opens a possibility of engineering heterostructures where  $(Bi_{1-x}In_x)_2Se_3$  layers with different In content and therefore

different band structures are seamlessly integrated to yield new functionalities. Specifically,  $(Bi_{1-x}In_x)_2Se_3$ , with In concentration in the trivial BI range can serve as a gate dielectric material or tunnel barrier between TI SS, essential components of TI field effect transistors, spin valves, topological tunnel junctions and other TI devices. Achieving those novel functionalities requires characterization of the electronic properties and ultrafast dynamics of intrinsic and optically excited carriers in  $(Bi_{1-x}In_x)_2Se_3$  over a large range of In concentrations.

The electronic band structure of  $Bi_2Se_3$  has been extensively investigated by angle-resolved photoemission spectroscopy (ARPES) and Shubnikov–de Haas measurements, which confirm the presence of spin-polarized Dirac SS that are well separated from the bulk states.  $^{2,7,12,19-22}$  In addition to these occupied SS, two-photon ARPES and time-resolved ARPES measurements with  $\sim 3$  eV excitation have uncovered addi-

Received: June 9, 2020 Published: September 14, 2020





tional, unoccupied Dirac SS located energetically  $\sim 1.5$  eV above the conduction band minimum and accessible by optical excitation. <sup>10,23</sup> In  $(\mathrm{Bi}_{1-x}\mathrm{In}_x)_2\mathrm{Se}_3$  with x>0, ARPES measurements confirmed that the system passes through a nontopological metallic state for  $x\sim 4\%$  and evolves into a trivial BI for  $x\geq 10\%$ .

In a TI state, it is difficult to disentangle the contribution of the SS states to room temperature electrical conductivity using conventional transport measurements. Most samples are n-doped due to the presence of Se vacancies and antisite defects, and the resulting bulk carrier conduction can overwhelm the SS contribution. The bulk carrier density in  $\rm Bi_2Se_3$  depends on growth kinetics, and can vary from very low values of  $\sim\!10^{17}$  cm $^{-3}$  to over  $10^{19}$  cm $^{-3}$ . In addition to finite bulk conduction, another topologically trivial transport channel that can obscure observation of SS conduction is the quantum well states (QWS) that can form in the 3–4 QLs immediately adjacent to the surfaces.  $^{11,21,27,28}$ 

Recently, investigation of the far-infrared complex optical conductivity of  $\rm Bi_2Se_3$  films using THz time-domain spectroscopy (TDS) allowed disambiguating contributions from SS, QWS, and bulk states. Establishing an important benchmark, authors showed that the mobility of carriers in the QWS is more than 50 times lower than that in the SS (54 cm²/(V·s) versus 2880 cm²/(V·s)). THz TDS studies have also mapped out the evolution of the optical conductivity in  $(\rm Bi_{1-x}In_x)_2Se_3$  over the sequential phase transitions from TI state to metallic and finally, trivial BI state as a function of In content from 0% to 25%.  $^{15,30,31}$ 

Finally, time-resolved techniques such as time-resolved ARPES, optical pump-optical probe spectroscopy with probe in the visible to mid-infrared range, time-resolved second harmonic generation (SHG), THz emission spectroscopy, as well as time-resolved THz spectroscopy (TRTS) have been used to uncover various aspects of optically excited carrier dynamics. 30,32-42 Of these techniques, optical pump-optical probe measurements are invaluable for probing interband processes, and time-resolved ARPES, time-resolved SHG and THz emission probe exclusively processes that occur at the surface. TRTS allows monitoring of the evolution of the complex optical conductivity in response to photoexcitation with subpicosecond time resolution, and is best suited for unraveling the dynamics of the photoexcited carriers as they interact with both the surface states and with the states in the bulk band structure. TRTS studies explored effects of the interaction of optically injected carriers with bulk and surface states, as well as with the bulk  $\alpha$ -phonon in Bi<sub>2</sub>Se<sub>3</sub>. <sup>34,41,43</sup>

In this study, our focus is on exploring how photoconductivity in  $(Bi_{1-x}In_x)_2Se_3$  evolves with In content increasing to 25% and 50%, well beyond the onset of the trivial BI phase.  $(Bi_{1-x}In_x)_2Se_3$  with x values above the BI threshold is ideally suitable for structurally compatible, tunable insulating layers for TI devices. 18 We use time-resolved THz spectroscopy with 800 nm (1.55 eV) and 400 nm (3.1 eV) excitation to study the dynamics of optically excited carriers in MBE-grown ~100QL (Bi<sub>1-x</sub>In<sub>x</sub>)<sub>2</sub>Se<sub>3</sub> films with x = 0, 0.25, and 0.5, on two sides of TI-BI transition. We establish that high photoinduced conductivity in Bi<sub>2</sub>Se<sub>3</sub> is dominated by free carriers that are excited into bulk conduction band but rapidly, over several picoseconds, scatter to the high mobility topological surface states. On the other hand, photoexcited carriers in indium-containing films have significantly lower carrier mobility that is sensitive to the indium concentration,

and experience weak confinement and suppressed long-range transport due to the twin domain boundaries and possible phase segregation. Indium concentration can thus be used to engineer carrier mobility, photoconductivity rise time, as well as the lifetime of optically injected carriers, tailoring the ultrafast response of  $(\mathrm{Bi}_{1-x}\mathrm{In}_x)_2\mathrm{Se}_3$  films for high speed optoelectronic devices, including TI/BI heterostructure devices.

#### **EXPERIMENTAL METHODS**

Growth of  $(Bi_{1-x}In_x)_2Se_3$  Thin Films.  $(Bi_{1-x}In_x)_2Se_3$  thin films on c-plane sapphire ( $\sim$ 0.5 mm thick) with three different compositions were grown by molecular beam epitaxy with a thickness of ~100 nm. Bismuth and indium fluxes were adjusted based on the beam equivalent pressure measured using a tungsten filament to achieve the desired compositions. The selenium flux was fixed during the growth and was maintained after the growth until the sample cooled below 200 °C to prevent selenium outgassing and vacancy formation. A cracker source for selenium was used to break the large selenium molecules into more reactive monomers and dimers which also helps reduce vacancy formation. A two-step growth method was adopted for the indium-containing films, which involves an initial seed-layer growth with the desired composition to maintain the correct phase and polytype. 17 Detailed thin film growth information has been reported elsewhere. 44,45 The AFM images of the resulting films are shown in Supporting Information, Figure S1. The image of Bi<sub>2</sub>Se<sub>3</sub> shows pyramidlike domains of ~500 nm size that have previously been attributed to twin domains.<sup>46</sup> The twin domains are mainly resulted from relative rotation (~60° in hexagonal symmetry) of growth front direction.<sup>44</sup> Both Incontaining films also show evidence of pyramidlike domains, though the domains are smaller. This is likely caused by the shorter diffusion length of indium adatoms compared to bismuth adatoms.

**THz Spectroscopy.** Equilibrium complex optical conductivity in  $(Bi_{1-x}In_x)_2Se_3$  films was explored using THz TDS in a transmission configuration. THz probe pulses with a bandwidth between 0.3 and 2.4 THz (1–10 meV) were generated by optical rectification of 800 nm, 100 fs pulses from a 1 kHz amplified Ti:sapphire laser in a 1 mm thick [110] ZnTe crystal and focused onto a  $\sim$ 1.5 mm diameter spot on the sample. The transmitted THz pulses were then coherently detected in a second ZnTe crystal by electro-optic sampling. Comparing, in the frequency domain, the amplitude and phase of THz pulses transmitted through the sapphire substrate allowed extraction of frequency-dependent complex conductivity.

Effects of optical excitation on the THz conductivity and photoexcited nonequilibrium carrier dynamics were investigated using TRTS, where either 800 nm (1.55 eV) or 400 nm (3.1 eV), 100 fs optical pulses were used to inject hot carriers. The photoinduced transient changes in the complex THz conductivity were interrogated using a time-delayed THz probe pulse. In the limit of small photoinduced changes, the negative change in the transmission of the THz probe pulse peak is proportional to the transient change in the conductance, or the photoconductance  $(-\Delta T(t)/T \propto \Delta G(t))$ .

### RESULTS AND DISCUSSION

Equilibrium Conductivity in  $(Bi_{1-x}ln_x)_2Se_3$  Films. The necessary first step to investigating the effects of optical excitation on the free carrier dynamics with TRTS is characterization of the equilibrium THz conductivity of the films using THz TDS. Measured complex THz TDS spectra are shown in Figure 1. For  $Bi_2Se_3$ , the observed spectrum is in

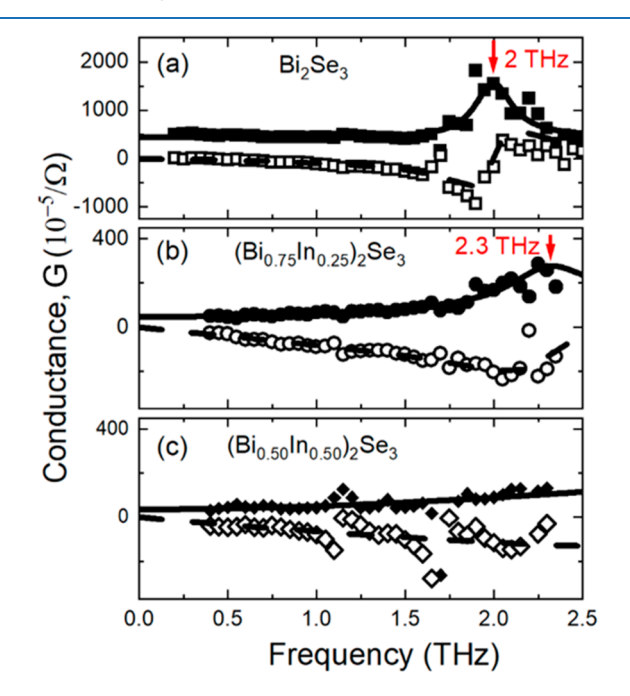


**Figure 1.** THz TDS spectra: Equilibrium conductance of  $(Bi_{1-x}In_x)_2Se_3$  films with x=0% (a), x=25% (b), and x=50% (c). Solid symbols represent real, and open symbols imaginary conductivity, with lines showing global fits of both the real and imaginary conductivity to the Drude–Lorentz model.

agreement with previous reports of THz sheet conductance. \$^{8,15,29,34,41} It exhibits a broad free carrier Drude response at low frequencies that can be extrapolated to a zero frequency, DC value  $G_{\rm DC} \sim (430 \pm 30) \times 10^{-5}~\Omega^{-1}$ . In addition to the low frequency Drude free carrier response, the THz complex conductivity of Bi<sub>2</sub>Se<sub>3</sub> exhibits a strong contribution of a bulk infrared-active in-plane  $\alpha$ -phonon mode at 2 THz (66.7 cm<sup>-1</sup>, or 8.3 meV).  $^{15,29,30,34}$  In the absence of a substantial interaction between the bulk phonon and topological SS, the phonon resonance is symmetric, and the overall complex conductance can be described by a Drude–Lorentz conductivity model which combines a Lorentzian to represent the phonon mode, and a free carrier Drude model to account for the free carrier response:

$$\begin{split} \tilde{G}(\omega) &= \tilde{G}_D(\omega) + \tilde{G}_{\text{Lorentz}}(\omega) \\ &= \left( \frac{\omega_p^2}{\Gamma_D - i\omega} + \frac{S_\alpha \omega (\Gamma_\alpha \omega - i(\omega_\alpha^2 - \omega^2))}{(\omega_\alpha^2 - \omega^2)^2 + (\Gamma_\alpha \omega)^2} \right) \varepsilon_0 d \end{split} \tag{1}$$

Here,  $\Gamma_D/2\pi$  is the Drude carrier scattering rate,  $((\omega_p/2\pi)^2d)$  is the 2D Drude spectral weight, with  $\omega_p/2\pi$  representing the plasma frequency,  $\varepsilon_0$  is the permittivity of free space, and d is the film thickness. Parameters of the Lorentzian contribution are the  $\alpha$ -phonon in THz,  $\omega_\alpha/2\pi$ , the phonon damping constant in THz,  $\Gamma_\alpha/2\pi$ , and  $S_\alpha$  which is its oscillator strength. This phonon mode broadens, with  $\Gamma_\alpha/2\pi$  increasing from  $\sim$ 0.25 to  $\sim$ 0.55 THz for x=25%. It also shifts to the higher energy due to lower atomic weight of In compared to Bi, appearing at  $\sim$ 2.3 THz for x=25%, in agreement with the previous observations. The for x=25% it shifts out of our probe bandwidth, appearing only as a broad positive real and negative imaginary conductance components, slowly increasing over the experimental spectral window.

The prominent phonon feature and high free carrier scattering rate resulting in a nearly flat free carrier response

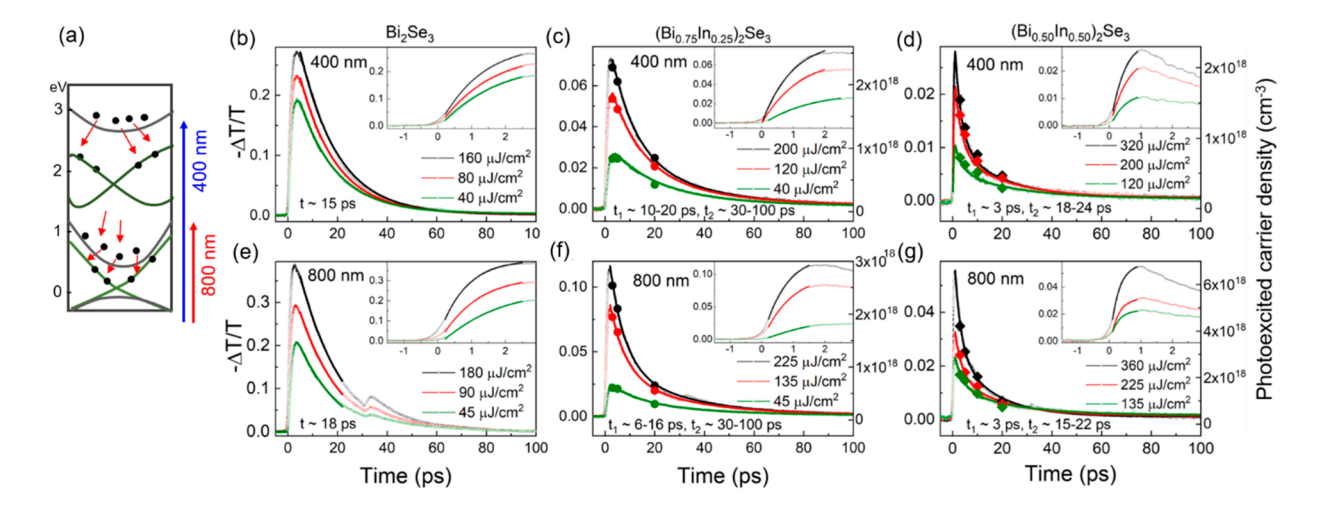


Figure 2. (a) Schematic illustrating the band structure of  $Bi_2Se_3$  with two sets of SS. Excitation with 800 nm pulses excites carriers into the lower states of the bulk CB above SS1, and 400 nm pulses can inject carriers into the higher lying states in CB above the SS2. Following excitation, the photoexcited electrons scatter from CB to SS. Transient change in THz  $(-\Delta T/T \propto \Delta \sigma)$  transmission of  $(Bi_{1-x}In_x)_2Se_3$  films as a function of time after photoexcitation with 400 nm (b-d) and 800 nm (e-g) pulses with excitation fluences indicated in the legends. Solid lines in (b-d) represent fits of  $-\Delta T/T$  decays to either a single exponential (b,e) or a double-exponential (c,d,f,g) decay functions with the decay times indicated in the panels. Insets show the same data zoomed around the photoconductivity rise, with solid lines showing singe-exponential rise fits. Second peaks seen in (e), (f), and (g) result from re-excitation by an 800 nm pulse reflected from substrate/air interface. In (c), (d), (f), (g), the solid symbols and the scale on the right represent photoexcited carrier density extracted from the Drude–Smith analysis of transient change in conductance.

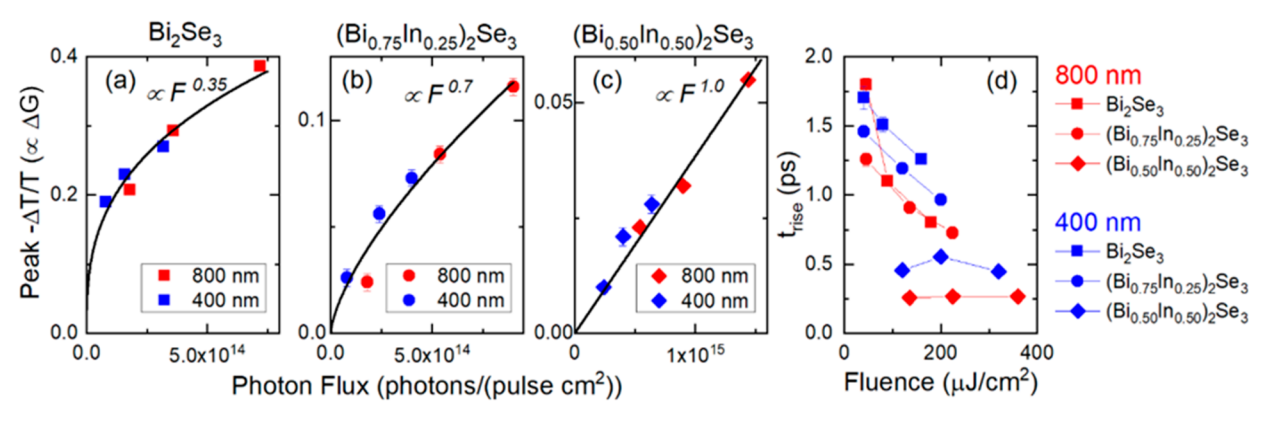


Figure 3. (a–c) Peak of  $-\Delta T/T$  at 800 and 400 nm as a function of the photon flux in an excitation pulse. Symbols show the experimental data, and solid lines show power law fits with fit results given in the panels. (d) Rise time of  $-\Delta T/T$  as a function of the excitation fluence of 800 and 400 nm pulses for all three films.

precludes us from using the fitting of experimental complex conductance spectra to estimate carrier scattering time or carrier density. We know from prior THz measurements that the Drude response of MBE-grown Bi<sub>2</sub>Se<sub>3</sub> films is insensitive to the film thickness (16-100 quintuple layers, QL) as the effect of bulk free carriers on equilibrium conductivity is negligible, 4' with 2D conduction channels (SS and QWS) playing a dominant role.44 While it is difficult to disambiguate the contributions of those two channels, we can use their combined sheet carrier density  $N \sim 3.32 \times 10^{13} \text{ cm}^{-2}$  and Hall effect mobility of  $\mu \sim 623~{\rm cm}^2/({\rm V\cdot s})$  reported earlier for a similarly prepared sample, <sup>44</sup> to estimate  $G_{\rm DC} = N\mu e \sim 330 \times$  $10^{-5} \Omega^{-1}$ , comparable to our extrapolated value (Figure 1(a)). For both In-containing films, GDC is nearly zero, as expected for the trivial BI, and in agreement with previous Hall measurements that found similar films to be electrically insulating.<sup>17</sup> If there is any bulk free carrier response due to residual doping in either of the films, it is small enough to be entirely obscured by the phonon contribution. Sharp discontinuities in spectra at frequencies ~1.1 and ~1.6 THz arise from absorption of THz probe pulses by the rotational transitions of water molecules in ambient air, and all conductivity fitting was weighted by the spectral amplitude of the reference THz pulse to ensure these artifacts do not affect experimental fitting parameters.

Nonequilibrium Photoexcited Carrier Dynamics in  $(Bi_{1-x}In_x)_2Se_3$  Films. Next, we investigate the effects of light excitation with energies 1.55 and 3.1 eV on electronic properties of  $(Bi_{1-x}In_x)_2Se_3$  films using TRTS. A simplified schematic of Bi<sub>2</sub>Se<sub>3</sub> band structure is shown in Figure 2(a). It includes, in addition to SS within the bulk band gap (SS<sub>1</sub>), a second set of unoccupied Dirac SS (SS<sub>2</sub>) located ~1.5-1.8 eV above the bulk CB edge. 10,23 We expect the excitation with 800 nm (1.55 eV) pulses to predominantly excite bulk free carriers into the lowest CB band, but excitation of carriers from the Fermi edge that is typically located at ~300-400 meV to the higher CB states is also possible. Higher energy 400 nm pulses, on the other hand, can couple directly to the higher energy bulk CB states above the high energy 2D Dirac SS<sub>2</sub>. For  $(Bi_{0.75}In_{0.25})_2Se_3$  and  $(Bi_{0.50}In_{0.50})_2Se_3$ , surface states are no longer present, and the (indirect) band gap increases to ~0.6 and ~0.85 eV, respectively, while the higher bulk states that give rise to the onset of direct optical transitions occur at  $\sim 1.5$ and ~1.8 eV, respectively.<sup>45</sup>

Transient dynamics of the photoexcited carriers are captured in  $-\Delta T/T$  traces, negative change in transmission of the THz probe peak as a function of time after photoexcitation (Figure 2(b-g)), which is proportional to the transient photoconductance  $\Delta G$ . We also summarize the peak values of  $-\Delta T/T$  for all three samples as a function of the photon flux Figure 3(a-c), and the photoconductance rise time as a function of excitation fluence, determined by fitting the early time dynamics to a single-exponential rise (Figure 3(d)).

Several salient features need to be highlighted. First, the transient photoconductance  $\Delta G$  in Bi<sub>2</sub>Se<sub>3</sub> is positive for both 400 and 800 nm excitation, for all studied fluences and times after excitation, contrary to a transient suppression of THz sheet conductance in thinner (<20 QL) films in prior studies. 34,41 Direct photoexcitation of SS, just like photoexcitation of carriers in graphene, results in their rapid thermalization and an emergence of a population of hot carriers subject to an increased scattering rate, which manifests in the conductivity reduction observed in these studies. In ~100 QL films studied here, photoexcitation primarily injects free electrons into the bulk conduction band (Figure 2(a)), and they scatter into the unoccupied SS after initially relaxing to the lower energies within the bulk CB. As a result, film conductance increases due to a transient increase in free carrier density. This effect overwhelms the expected reduction in conductance due to direct excitation of SS.

Second, the peak transient increase in conductance is significantly higher in Bi<sub>2</sub>Se<sub>3</sub> compared to both In-containing films, for comparable or even lower excitation fluence values. This indicates that SS, characterized by significantly higher carrier mobility values than the bulk states, or even the QWS, determine the photoinduced response of Bi<sub>2</sub>Se<sub>3</sub>. Rather than exciting them directly, excitation with high photon energies of 1.55 and 3.1 eV injects carriers into the bulk conduction band, with 3.1 eV photons even accessing the second conduction band states. Those free carriers then scatter into the SS via phonon-assisted relaxation, as was observed previously in TRTS and TR-ARPES. 36,41 This relaxation occurs over few picoseconds, and is responsible for a rather slow buildup of photoinduced conductance in Bi<sub>2</sub>Se<sub>3</sub>, as can be seen in insets of Figure 2(b,e), as well as in the plot of the rise time as a function of excitation fluence (Figure 3(d)). Dependence of the peak  $-\Delta T/T$  as a function of the photon flux (e.g., number of incident photons per unit area of the sample in an excitation pulse) for both 800 and 400 nm excitation is shown in Figure

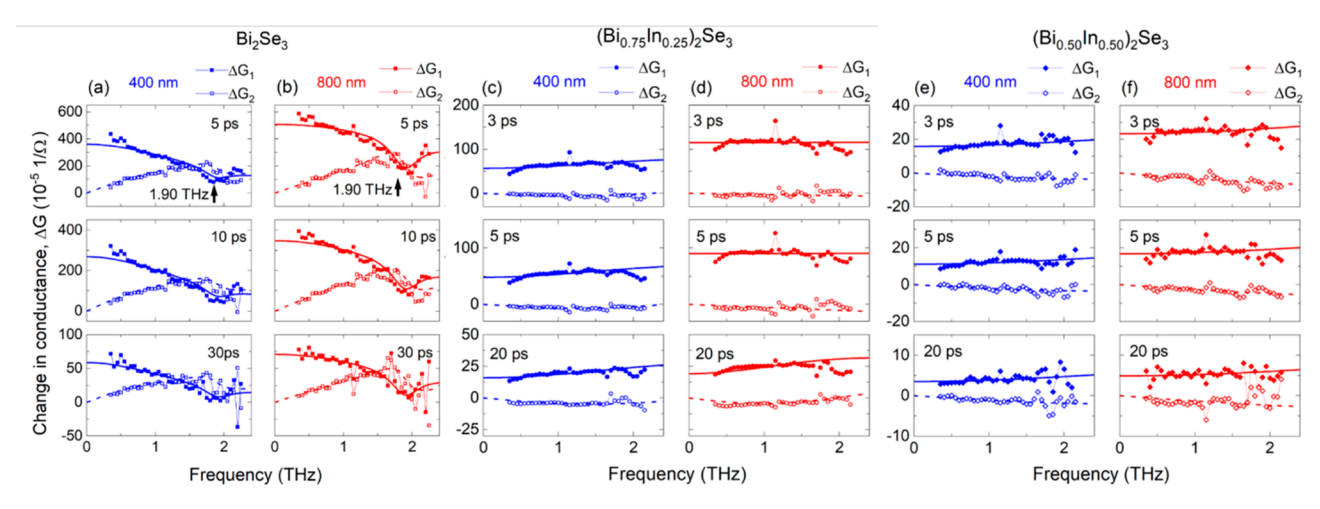


Figure 4. Photoinduced change in THz conductance in  $(Bi_{1-x}In_x)_2Se_3$  films at different times after excitation with fluences of 200  $\mu$ J/cm² for 400 nm (shown in blue) and 225  $\mu$ J/cm² for 800 nm (shown in red). Solid and open symbols indicate the real  $(\Delta G_1)$  and imaginary  $(\Delta G_2)$  components of the transient conductance change. Solid and dashed lines are global fits of  $\Delta G_1$  and  $\Delta G_2$  to a Drude–Lorentz model (eq 1) for  $Bi_2Se_3$ , and the Drude–Smith model (eq 2) for  $(Bi_0.75In_{0.25})_2Se_3$  and  $(Bi_{0.50}In_{0.50})_2Se_3$ .

3(a-c), where the solid lines are power law fits. For each film, peak photoconductance values for both 800 and 400 nm excitation fall on the same curves, indicating that each absorbed photon contributes one electron—hole pair to the photoinduced response. For  $Bi_2Se_3$ , the peak photoinduced change in conductance saturates with increased excitation, as indicated by the power law exponent  $\sim 0.35$  (Figure 3(a)). Saturation occurs as a result of filling of the SS bands. Higher excitation fluences reduce the observed photoconductance rise time. Carrier—carrier scattering at high fluences also plays a role of an additional relaxation channel, accelerating scattering toward the SS. Finally, the rise time for most fluence values appear to be slower for 400 nm excitation, likely an indication of the slower scattering of bulk carriers to  $SS_2$ .

Interestingly, the peak also shows signs of saturation behavior indicated by a power law exponent of ~0.7 (Figure 3(b)), albeit weaker, for  $(Bi_{0.75}In_{0.25})_2Se_3$ , but not for  $(Bi_{0.50}In_{0.50})_2Se_3$ , although for x = 50%, the peak does not reach the range where saturation sets in for x = 25%, even at higher excitation photon flux. (Bi<sub>0.75</sub>In<sub>0.25</sub>)<sub>2</sub>Se<sub>3</sub> film also exhibits a fluence dependent rise time, comparable to that of Bi<sub>2</sub>Se<sub>3</sub>. For (Bi<sub>0.50</sub>In<sub>0.50</sub>)<sub>2</sub>Se<sub>3</sub> film, rise time is short and not dependent on fluence, ~260 fs for 800 nm excitation, and ~500 fs for 400 nm excitation. Carriers in both In-containing films are still excited well above the CB minimum. Many of them rapidly become trapped by bulk defect states or trap states associated with the twin boundaries over the time scales beyond our experimental time resolution (<200 fs). In the absence of SS, the remaining carriers likely scatter into lowerlying, higher mobility bands. Filling and emptying of those higher mobility CB states may lead to a relaxation bottleneck, observed as a slow rise time in  $(Bi_{0.75}In_{0.25})_2Se_3$  at low excitation fluence values. As increased fluence leads to a higher instantaneous carrier density, carrier-carrier scattering processes contribute to accelerated relaxation. We also hypothesize that higher density of trap states, combined with a lower excess energy of the photoexcited carriers due to the higher energies of CB states in  $(Bi_{0.50}In_{0.50})_2Se_3$  compared to (Bi<sub>0.75</sub>In<sub>0.25</sub>)<sub>2</sub>Se<sub>3</sub>, make trapping a much faster process and preclude observation of appreciable band filling effects that manifest as a slow rise.

After photoinduced transient conductance reaches a peak, it decays within tens of picoseconds. In Bi<sub>2</sub>Se<sub>3</sub>, the SS photoconductivity decays to zero with 15–18 ps time constant. In both In-containing films, on the other hand, photoconductivity follows a two-exponential decay, indicating the presence of at least two carrier-trapping mechanisms that may involve trap states associated with the bulk disorder due to In substitutions, possible phase segregation and nonuniform indium concentration throughout the film, as well as twin boundaries. Both decay components are significantly shorter in x = 50% film (3 ps vs 6–20 ps, and ~20 ps vs 30–100 ps), indicating that In concentration can be used to tailor ultrafast response in  $(Bi_{1-x}In_x)_2Se_3$  trivial BIs for applications in highspeed devices.

We can get a much more detailed picture of the transient changes in conductance by examining the excitation-induced changes to the complex, frequency-resolved conductance at different times after the arrival of the optical pump pulse. Examples of those spectra for 400 and 800 nm excitation for all three films are given in Figure 4.

Again, the spectra for Bi<sub>2</sub>Se<sub>3</sub> are dramatically different compared to those for  $(Bi_{0.75}In_{0.25})_2Se_3$  and  $(Bi_{0.50}In_{0.50})_2Se_3$ : not only is the transient change in conductance about an order of magnitude stronger for the same excitation fluence values in TI phase, and the spectral shape differs drastically for it from those in In-containing films. Like the equilibrium conductance, the transient conductance of Bi<sub>2</sub>Se<sub>3</sub> exhibits a pronounced Drude free carrier response, described by the first term of eq 1, at low frequencies, which we attribute to the photoexcited carriers scattered to SS states. In (Bi<sub>0.75</sub>In<sub>0.25</sub>)<sub>2</sub>Se<sub>3</sub> and (Bi<sub>0.50</sub>In<sub>0.50</sub>)<sub>2</sub>Se<sub>3</sub>, the real photoinduced conductance component  $\Delta G_1$  that increases with increasing frequency and negative imaginary photoinduced conductance  $\Delta G_2$  are indicative of the effects of disorder and backscattering of charge carriers that are typically observed in nanostructured and granular materials. The potential phase segregation and nonuniform indium distribution, as well as the twin domain boundaries that act not only as carrier trapping sites but also as partially transparent boundaries, both may be contributing to localization of free optically excited bulk carriers over mesoscopic length scales. The THz complex conductivity of such systems can be welldescribed by a Drude-Smith model, a phenomenological

extension to the Drude model where an additional parameter  $(-1 \le c \le 0)$  accounts for the effects of disorder and localization within the grains or domains, as grain boundaries impede long-range transport and thus suppress conductivity at low frequencies. <sup>48–56</sup> In this model, the transient change of complex film conductance is given by

$$\Delta G_{DS} = \frac{\omega_p^2 \varepsilon_0 \tau_{DS}}{(1 - i\omega \tau_{DS})} \left( 1 + \frac{c}{1 - i\omega \tau_{DS}} \right) d \tag{2}$$

where  $au_{DS}$  is carrier scattering time (related to the corresponding scattering rate as  $2\pi\Gamma_{DS} = 1/\tau_{DS}$ ). When c =0, the Drude model is recovered, and when c = -1, carrier localization over the short distances leads to a complete suppression of conductivity at  $\omega = 0$ . The lines in Figure 4(cf) are the global fits on the complex change in conductance to eq 2. In the absence of highly conductive SS, bulk volume carrier density N can be calculated from the plasma frequency as  $=\frac{\omega_p^2 \varepsilon_0 m^*}{e^2}$ , where  $m^*$  is the carrier effective mass which we take here to be 0.15  $m_e^{-7.8}$  Time- and excitation-dependent instantaneous photoexcited carrier density values obtained from fitting the frequency-resolved complex photoconductance spectra of x = 25% and x = 50% films at 3, 5, and 20 ps are shown alongside the  $-\Delta T/T$  decays in Figure 2(c-g). We find that the photoconductivity decay tracks photoexcited carrier density for all excitation fluence values. Using those values to estimate the photoexcited carrier density that corresponds to the peak photoconductivity, and comparing it to the total injected carrier density estimated from the photon flux, we find that only 3-5% of all carriers contributed to the observed photoconductivity, while the vast majority are lost to rapid

The *c*-parameter values for In-containing films at different excitation fluence values and times after excitation are shown in Figure 5. In both samples, localization of carriers over mesoscopic length scales is pronounced, and the effect is stronger in x = 50% film. We also find that the c parameter becomes slightly more negative with time after excitation, going from  $\sim$ -0.55-0.65 to  $\sim$ -0.7 in  $(Bi_{0.75}In_{0.25})_2Se_3$ , and from  $\sim$ -0.7 to  $\sim$ -0.8 in  $(Bi_{0.50}In_{0.50})_2Se_3$ . Such behavior of

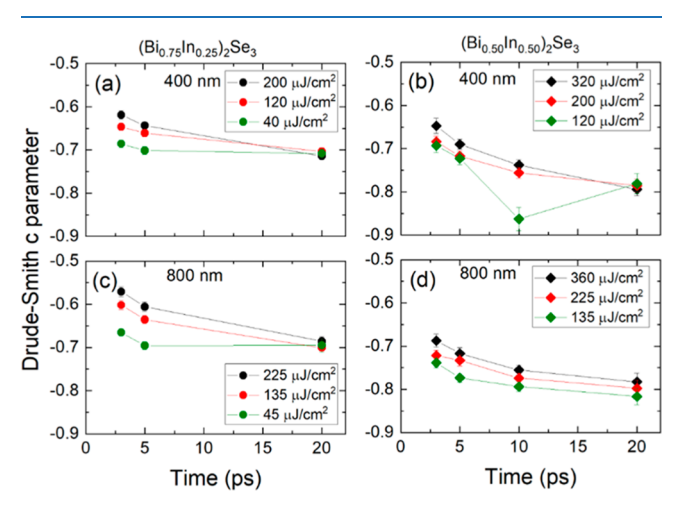


**Figure 5.** Time evolution of the Drude–Smith c parameter for photoexcited charge carriers in  $(\mathrm{Bi}_{1-x}\mathrm{In}_x)_2\mathrm{Se}_3$  films with x=25% and x=50% for 400 nm (a,b) and 800 nm (c,d) excitation. Excitation fluence values are given in legends.

photoinjected carriers has been reported in many other semiconductors and insulators, where crystalline regions are separated by the grain or domain boundaries. S2,53,55 Carriers become more affected by localization as they thermalize with the lattice. Lower localization at the early times experienced by the carriers excited by 400 nm pulses compared to 800 nm pulses supports this hypothesis. It may be also possible that as carriers get trapped at bulk defects and domain boundaries, they may impact long-range transport of the remaining free carriers. Excitation fluence also impacts average carrier localization, as injecting more carriers appears to result in slightly less obstructed long-range transport at early times, likely as higher injected hot carrier density takes longer to thermalize with the crystal lattice by emission of phonons.

Finally, using the experimental Drude–Smith parameters  $\tau_{DS}$  and c, we can also estimate short-range and long-range carrier mobility for photoexcited bulk free carriers as  $\mu_{\text{short-range}} = \frac{e \tau_{DS}}{m^*}$  and  $\mu_{\text{long-range}} = \mu_{\text{short-range}} (1 + c)$ . The summary of the  $\tau_{DS}$  values is given in Table 1.

Table 1. Drude–Smith  $\tau_{DS}$  Values for x=25% and x=50% Films, Obtained by Fitting Photoconductivity Spectra to Eq. 2.

	$(Bi_{0.75}In_{0.25})_2Se_3$	$(Bi_{0.5}In_{0.5})_2Se_3$
$ au_{DS}$ (400 nm)	$35 \pm 7 \text{ fs}$	$20 \pm 10 \text{ fs}$
$ au_{DS}~(800~\mathrm{nm})$	$50 \pm 10 \text{ fs}$	$15 \pm 5 \text{ fs}$

We find for  $(Bi_{0.75}In_{0.25})_2Se_3$ , that  $\mu_{short\text{-range}}$  describing carrier motion over the short distance within individual domains is in  $400-600 \text{ cm}^2/(\text{V}\cdot\text{s})$  range. Mobility over macroscopic distances,  $\mu_{long\text{-range}}$  is as high as  $180-270 \text{ cm}^2/(\text{V}\cdot\text{s})$  at early times, and decreases to  $120-180 \text{ cm}^2/(\text{V}\cdot\text{s})$  at later times as the stronger carrier localization sets in. For  $(Bi_{0.50}In_{0.50})_2Se_3$ ,  $\mu_{short\text{-range}} \sim 200 \text{ cm}^2/(\text{V}\cdot\text{s})$ , and  $\mu_{long\text{-range}}$  decreased over time from  $60 \text{ cm}^2/(\text{V}\cdot\text{s})$  to  $40 \text{ cm}^2/(\text{V}\cdot\text{s})$ . This demonstrates that varying indium content allows fabrication of  $(Bi_{1-x}In_x)_2Se_3$  films with different lifetimes as well as mobilities of optically excited carriers, thus tailoring the properties for a specific application.

Returning to Bi<sub>2</sub>Se<sub>3</sub>, we find that photoexcited carriers exhibit a Drude response with c = 0, as SS are not susceptible to backscattering. In addition to the free carrier response, we observe excitation-induced blue-shift of the  $\alpha$ -phonon, which presents as a negative Lorentzian contribution in the differential conductance  $\Delta G$ . Such change of the  $\alpha$ -phonon frequency has been reported in prior studies and attributed to a change in lattice temperature that results from thermalization of optically injected hot carriers. <sup>34,41</sup> The lines in Figure 4(a,b) represent global fits of the real and imaginary parts of the differential conductance  $\Delta G$  to eq 1 with negative time- and fluence-dependent Lorentzian amplitude  $S_{\alpha}$ , and a damping rate  $\Gamma_{\alpha}/2\pi \sim 0.45$  THz. From the fitting, we obtain both the 2D Drude spectral weight and the Drude scattering rate. We find that, for each excitation wavelength, the scattering rate appears to be a function of the Drude spectral weight, suggesting that carrier-carrier scattering is a limiting factor on carrier mobility ( $\mu \propto \tau_D \propto 1/\Gamma_D$ ). Data in Figure 6 also show that the scattering rate is significantly lower for the carriers excited with 400 nm, indicating the difference in properties of the two sets of SS, SS<sub>1</sub> which becomes populated following excitation with 800 nm pulses, and SS<sub>2</sub>, which is accessible to

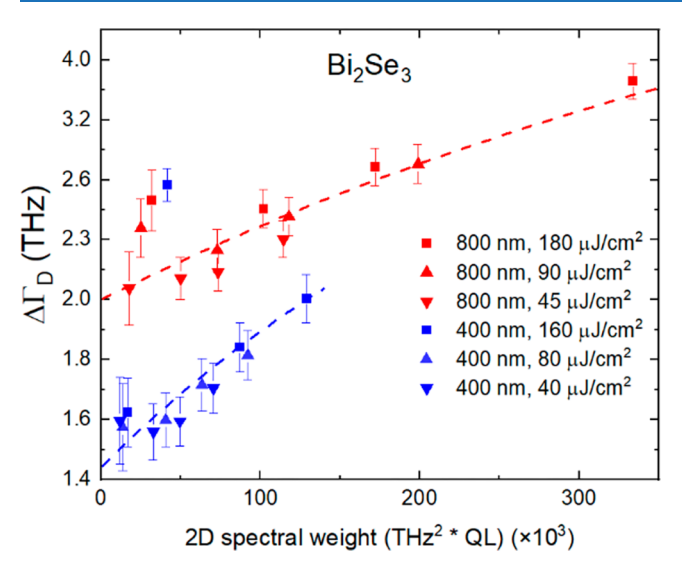


Figure 6. Scattering rate  $\Gamma_D$  as a function of photoexcited 2D Drude spectral weight in Bi<sub>2</sub>Se<sub>3</sub> at different times after photoexcitation with 800 and 400 nm. Lines are guides to the eye.

carriers injected higher into the CB by 400 nm pulses (Figure 2(a)). Finally, we note here that the scattering times  $\tau_{D}$ , corresponding to the lower carrier density limit, are  $\sim$ 100 fs for SS<sub>1</sub>, and  $\sim$ 80 fs for SS<sub>2</sub>. Taking the effective mass in the SS to be 0.07  $m_e$ , <sup>29</sup> we estimate the corresponding carrier mobility values to be  $\sim$ 2500 cm<sup>2</sup>/(V·s) and  $\sim$ 2000 cm<sup>2</sup>/(V·s).

In conclusion, we have studied nonequilibrium dynamics of photoexcited free carriers in three ~100 QL thick, MBE-grown  $(Bi_{1-x}In_x)_2Se_3$  films with x = 0, 25%, and 50%, representing the end points of topological insulator-metal-insulator phase transition that occur as the indium concentration is increased. Excitation of charge carriers with 1.5 eV (800 nm) and 3.1 eV (400 nm) pulses allowed investigation of the carriers injected into different energy levels of the conduction band. We find that in the TI limit, topological surface states dominate both equilibrium and nonequilibrium properties. Carriers that are optically injected into the bulk conduction band relax to the surface states over few picoseconds, where they exhibit high carrier mobility and are not susceptible to scattering by the twin domain boundaries present in the film. We also find that photoexcited carriers in the second set of Dirac surface states, located ~1.5-1.8 eV above the conduction band minimum and accessible by 3.1 eV excitation, experience lower scattering and have higher mobility than those in the lower-lying surface states within the band gap. For indium-containing films, we find that photoexcitation generates bulk free carriers that experience partial localization over mesoscopic length scales, commensurate with the presence of the twin domain boundaries. Dynamics of the photoexcited carriers in Incontaining  $(Bi_{1-x}In_x)_2Se_3$  films, including both the rise time of photoconductivity and the carrier lifetime, depend on In concentration, demonstrating that specific properties desired for high-speed photonic devices can be achieved by composition engineering of  $(Bi_{1-x}In_x)_2Se_3$ . As insulating  $(Bi_{1-x}In_x)_2Se_3$  is structurally compatible with TI  $Bi_2Se_3$ , the ability to tune its optoelectronic properties makes it highly desirable for applications in high-speed optical, electronic, and spintronic devices based on TI/BI heterostructures.

# ASSOCIATED CONTENT

# Supporting Information

The Supporting Information is available free of charge at https://pubs.acs.org/doi/10.1021/acsphotonics.0c00928.

Figure S1: AFM micrographs of the studied films (PDF)

## AUTHOR INFORMATION

### **Corresponding Authors**

Teng Shi — Department of Physics, Worcester Polytechnic Institute, Worcester, Massachusetts 01609, United States; Email: tshi@wpi.edu

Lyubov V. Titova — Department of Physics, Worcester Polytechnic Institute, Worcester, Massachusetts 01609, United States; oorcid.org/0000-0002-2146-9102; Email: ltitova@ wpi.edu

#### **Authors**

Kateryna Kushnir – Department of Physics, Worcester Polytechnic Institute, Worcester, Massachusetts 01609, United States

**Zhengtianye Wang** — Department of Materials Science and Engineering, University of Delaware, Newark, Delaware 19716, United States

Stephanie Law — Department of Materials Science and Engineering, University of Delaware, Newark, Delaware 19716, United States; Ocid.org/0000-0002-5087-6663

Complete contact information is available at: https://pubs.acs.org/10.1021/acsphotonics.0c00928

#### Notes

The authors declare no competing financial interest.

### ACKNOWLEDGMENTS

T.S., K.K., and L.V.T. acknowledge support from the National Science Foundation DMR-1750944. Z.W. and S.L. acknowledge support from the U.S. Department of Energy (DOE), Office of Science, Office of Basic Energy Sciences under Award No. DE-SC0017801. Z.W. and S.L. also acknowledge the use of the Materials Growth Facility (MGF) at the University of Delaware, which is partially supported by the National Science Foundation Major Research Instrumentation under Grant No. 1828141 and is a member of the Delaware Institute for Materials Research (DIMR).

## REFERENCES

- (1) Moore, J. E. The birth of topological insulators. *Nature* **2010**, 464 (7286), 194–198.
- (2) Xia, Y.; Qian, D.; Hsieh, D.; Wray, L.; Pal, A.; Lin, H.; Bansil, A.; Grauer, D.; Hor, Y. S.; Cava, R. J.; Hasan, M. Z. Observation of a large-gap topological-insulator class with a single Dirac cone on the surface. *Nat. Phys.* **2009**, *5* (6), 398–402.
- (3) Qi, X.-L.; Zhang, S.-C. Topological insulators and superconductors. Rev. Mod. Phys. 2011, 83 (4), 1057–1110.
- (4) Zhang, X.; Wang, J.; Zhang, S.-C. Topological insulators for high-performance terahertz to infrared applications. *Phys. Rev. B: Condens. Matter Mater. Phys.* **2010**, 82 (24), 245107.
- (5) Pesin, D.; MacDonald, A. H. Spintronics and pseudospintronics in graphene and topological insulators. *Nat. Mater.* **2012**, *11* (5), 409–416.
- (6) Peng, H.; Dang, W.; Cao, J.; Chen, Y.; Wu, D.; Zheng, W.; Li, H.; Shen, Z.-X.; Liu, Z. Topological insulator nanostructures for near-infrared transparent flexible electrodes. *Nat. Chem.* **2012**, *4* (4), 281–286.

- (7) Analytis, J. G.; Chu, J.-H.; Chen, Y.; Corredor, F.; McDonald, R. D.; Shen, Z. X.; Fisher, I. R. Bulk Fermi surface coexistence with Dirac surface state in Bi<sub>2</sub>Se<sub>3</sub>: A comparison of photoemission and Shubnikov-de Haas measurements. *Phys. Rev. B: Condens. Matter Mater. Phys.* **2010**, *81* (20), 205407.
- (8) Butch, N. P.; Kirshenbaum, K.; Syers, P.; Sushkov, A. B.; Jenkins, G. S.; Drew, H. D.; Paglione, J. Strong surface scattering in ultrahighmobility B<sub>2</sub>Se<sub>3</sub> topological insulator crystals. *Phys. Rev. B: Condens. Matter Mater. Phys.* **2010**, *81* (24), 241301.
- (9) Ghaemi, P.; Mong, R. S. K.; Moore, J. E. In-Plane Transport and Enhanced Thermoelectric Performance in Thin Films of the Topological Insulators Bi<sub>2</sub>Te<sub>3</sub> and Bi<sub>2</sub>Se<sub>3</sub>. *Phys. Rev. Lett.* **2010**, *105* (16), 166603.
- (10) Soifer, H.; Gauthier, A.; Kemper, A. F.; Rotundu, C. R.; Yang, S. L.; Xiong, H.; Lu, D.; Hashimoto, M.; Kirchmann, P. S.; Sobota, J. A.; Shen, Z. X. Band-Resolved Imaging of Photocurrent in a Topological Insulator. *Phys. Rev. Lett.* **2019**, 122 (16), 167401.
- (11) de Vries, E. K.; Pezzini, S.; Meijer, M. J.; Koirala, N.; Salehi, M.; Moon, J.; Oh, S.; Wiedmann, S.; Banerjee, T. Coexistence of bulk and surface states probed by Shubnikov-de Haas oscillations in Bi<sub>2</sub>Se<sub>3</sub> with high charge-carrier density. *Phys. Rev. B: Condens. Matter Mater. Phys.* **2017**, *96* (4), No. 045433.
- (12) Zhang, H.; Liu, C.-X.; Qi, X.-L.; Dai, X.; Fang, Z.; Zhang, S.-C. Topological insulators in Bi<sub>2</sub>Se<sub>3</sub>, Bi<sub>2</sub>Te<sub>3</sub> and Sb<sub>2</sub>Te<sub>3</sub> with a single Dirac cone on the surface. *Nat. Phys.* **2009**, *5* (6), 438–442.
- (13) Brahlek, M.; Bansal, N.; Koirala, N.; Xu, S.-Y.; Neupane, M.; Liu, C.; Hasan, M. Z.; Oh, S. Topological-Metal to Band-Insulator Transition in (Bi<sub>1-x</sub>In<sub>x</sub>)<sub>2</sub>Se<sub>3</sub> Thin Films. *Phys. Rev. Lett.* **2012**, *109* (18), 186403.
- (14) Salehi, M.; Shapourian, H.; Koirala, N.; Brahlek, M. J.; Moon, J.; Oh, S. Finite-Size and Composition-Driven Topological Phase Transition in  $(Bi_{1-x}In_x)_2Se_3$  Thin Films. *Nano Lett.* **2016**, *16* (9), 5528–5532.
- (15) Wu, L.; Brahlek, M.; Valdés Aguilar, R.; Stier, A. V.; Morris, C. M.; Lubashevsky, Y.; Bilbro, L. S.; Bansal, N.; Oh, S.; Armitage, N. P. A sudden collapse in the transport lifetime across the topological phase transition in  $(Bi_{1-x}In_x)_2Se_3$ . *Nat. Phys.* **2013**, *9*, 410. Supplementary Information: https://www.nature.com/articles/nphys2647#supplementary-information.
- (16) Sánchez-Barriga, J.; Aguilera, I.; Yashina, L. V.; Tsukanova, D. Y.; Freyse, F.; Chaika, A. N.; Callaert, C.; Abakumov, A. M.; Hadermann, J.; Varykhalov, A.; Rienks, E. D. L.; Bihlmayer, G.; Blügel, S.; Rader, O. Anomalous behavior of the electronic structure of (Bi<sub>1-x</sub>In<sub>x</sub>)<sub>2</sub>Se<sub>3</sub> across the quantum phase transition from topological to trivial insulator. *Phys. Rev. B: Condens. Matter Mater. Phys.* **2018**, 98 (23), 235110.
- (17) Wang, Y.; Ginley, T. P.; Law, S. Growth of high-quality Bi<sub>2</sub>Se<sub>3</sub> topological insulators using (Bi<sub>1-x</sub>In<sub>x</sub>)<sub>2</sub>Se<sub>3</sub> buffer layers. *J. Vac. Sci. Technol., B: Nanotechnol. Microelectron.: Mater., Process., Meas., Phenom.* **2018**, 36 (2), No. 02D101.
- (18) Brahlek, M. J.; Koirala, N.; Liu, J.; Yusufaly, T. I.; Salehi, M.; Han, M.-G.; Zhu, Y.; Vanderbilt, D.; Oh, S. Tunable inverse topological heterostructure utilizing (Bi<sub>1-x</sub>In<sub>x</sub>)<sub>2</sub>Se<sub>3</sub> and multichannel weak-antilocalization effect. *Phys. Rev. B: Condens. Matter Mater. Phys.* **2016**, 93 (12), 125416.
- (19) Pan, Z. H.; Vescovo, E.; Fedorov, A. V.; Gardner, D.; Lee, Y. S.; Chu, S.; Gu, G. D.; Valla, T. Electronic Structure of the Topological Insulator Bi<sub>2</sub>Se<sub>3</sub> Using Angle-Resolved Photoemission Spectroscopy: Evidence for a Nearly Full Surface Spin Polarization. *Phys. Rev. Lett.* **2011**, *106* (25), 257004.
- (20) Neupane, M.; Richardella, A.; Sánchez-Barriga, J.; Xu, S.; Alidoust, N.; Belopolski, I.; Liu, C.; Bian, G.; Zhang, D.; Marchenko, D.; Varykhalov, A.; Rader, O.; Leandersson, M.; Balasubramanian, T.; Chang, T.-R.; Jeng, H.-T.; Basak, S.; Lin, H.; Bansil, A.; Samarth, N.; Hasan, M. Z. Observation of quantum-tunnelling-modulated spin texture in ultrathin topological insulator Bi<sub>2</sub>Se<sub>3</sub> films. *Nat. Commun.* **2014**, *5* (1), 3841.
- (21) Bianchi, M.; Guan, D.; Bao, S.; Mi, J.; Iversen, B. B.; King, P. D. C.; Hofmann, P. Coexistence of the topological state and a two-

- dimensional electron gas on the surface of Bi<sub>2</sub>Se<sub>3</sub>. Nat. Commun. 2010, 1 (1), 128.
- (22) Lu, H.-Z.; Shan, W.-Y.; Yao, W.; Niu, Q.; Shen, S.-Q. Massive Dirac fermions and spin physics in an ultrathin film of topological insulator. *Phys. Rev. B: Condens. Matter Mater. Phys.* **2010**, *81* (11), 115407.
- (23) Sobota, J. A.; Yang, S. L.; Kemper, A. F.; Lee, J. J.; Schmitt, F. T.; Li, W.; Moore, R. G.; Analytis, J. G.; Fisher, I. R.; Kirchmann, P. S.; Devereaux, T. P.; Shen, Z. X. Direct Optical Coupling to an Unoccupied Dirac Surface State in the Topological Insulator Bi<sub>2</sub>Se<sub>3</sub>. *Phys. Rev. Lett.* **2013**, *111* (13), 136802.
- (24) Lou, R.; Liu, Z.; Jin, W.; Wang, H.; Han, Z.; Liu, K.; Wang, X.; Qian, T.; Kushnirenko, Y.; Cheong, S.-W.; Osgood, R. M.; Ding, H.; Wang, S. Sudden gap closure across the topological phase transition in Bi<sub>2-x</sub>In<sub>x</sub>Se<sub>3</sub>. *Phys. Rev. B: Condens. Matter Mater. Phys.* **2015**, 92 (11), 115150.
- (25) Dai, J.; West, D.; Wang, X.; Wang, Y.; Kwok, D.; Cheong, S. W.; Zhang, S. B.; Wu, W. Toward the Intrinsic Limit of the Topological Insulator Bi<sub>2</sub>Se<sub>2</sub>. *Phys. Rev. Lett.* **2016**, *117* (10), 106401.
- (26) Unzueta, I.; Zabala, N.; Marín-Borrás, V.; Muñoz-Sanjosé, V.; García, J. A.; Plazaola, F. Observation of a charge delocalization from Se vacancies in Bi<sub>2</sub>Se<sub>3</sub>: A positron annihilation study of native defects. *Phys. Rev. B: Condens. Matter Mater. Phys.* **2016**, *94* (1), No. 014117.
- (27) Veyrat, L.; Iacovella, F.; Dufouleur, J.; Nowka, C.; Funke, H.; Yang, M.; Escoffier, W.; Goiran, M.; Eichler, B.; Schmidt, O. G.; Büchner, B.; Hampel, S.; Giraud, R. Band Bending Inversion in Bi<sub>2</sub>Se<sub>3</sub> Nanostructures. *Nano Lett.* **2015**, *15* (11), 7503–7507.
- (28) Bahramy, M. S.; King, P. D. C.; de la Torre, A.; Chang, J.; Shi, M.; Patthey, L.; Balakrishnan, G.; Hofmann, P.; Arita, R.; Nagaosa, N.; Baumberger, F. Emergent quantum confinement at topological insulator surfaces. *Nat. Commun.* **2012**, *3* (1), 1159.
- (29) Park, B. C.; Kim, T. H.; Sim, K. I.; Kang, B.; Kim, J. W.; Cho, B.; Jeong, K. H.; Cho, M. H.; Kim, J. H. Terahertz single conductance quantum and topological phase transitions in topological insulator Bi<sub>2</sub>Se<sub>3</sub> ultrathin films. *Nat. Commun.* **2015**, DOI: 10.1038/ncomms7552.
- (30) Sim, S.; Koirala, N.; Brahlek, M.; Sung, J. H.; Park, J.; Cha, S.; Jo, M.-H.; Oh, S.; Choi, H. Tunable Fano quantum-interference dynamics using a topological phase transition in  $(Bi_{1-x}In_x)_2Se_3$ . *Phys. Rev. B: Condens. Matter Mater. Phys.* **2015**, *91* (23), 235438.
- (31) Zhu, J.; Liu, F.; Zhou, S.; Franke, C.; Wimmer, S.; Volobuev, V. V.; Springholz, G.; Pashkin, A.; Schneider, H.; Helm, M. Lattice vibrations and electrical transport in  $(Bi_{1-x}In_x)_2Se_3$  films. *Appl. Phys. Lett.* **2016**, *109* (20), 202103.
- (32) Glinka, Y. D.; Babakiray, S.; Johnson, T. A.; Bristow, A. D.; Holcomb, M. B.; Lederman, D. Ultrafast carrier dynamics in thinfilms of the topological insulator Bi<sub>2</sub>Se<sub>3</sub>. *Appl. Phys. Lett.* **2013**, *103* (15), 151903.
- (33) Glinka, Y. D.; Babakiray, S.; Johnson, T. A.; Holcomb, M. B.; Lederman, D. Effect of carrier recombination on ultrafast carrier dynamics in thin films of the topological insulator Bi<sub>2</sub>Se<sub>3</sub>. *Appl. Phys. Lett.* **2014**, *105* (17), 171905.
- (34) Valdés Aguilar, R.; Qi, J.; Brahlek, M.; Bansal, N.; Azad, A.; Bowlan, J.; Oh, S.; Taylor, A. J.; Prasankumar, R. P.; Yarotski, D. A. Time-resolved terahertz dynamics in thin films of the topological insulator Bi<sub>2</sub>Se<sub>3</sub>. *Appl. Phys. Lett.* **2015**, *106* (1), No. 011901.
- (35) Jnawali, G.; Linser, S.; Shojaei, I. A.; Pournia, S.; Jackson, H. E.; Smith, L. M.; Need, R. F.; Wilson, S. D. Revealing Optical Transitions and Carrier Recombination Dynamics within the Bulk Band Structure of Bi<sub>2</sub>Se<sub>3</sub>. *Nano Lett.* **2018**, *18* (9), 5875–5884.
- (36) Sobota, J. A.; Yang, S.; Analytis, J. G.; Chen, Y. L.; Fisher, I. R.; Kirchmann, P. S.; Shen, Z. X. Ultrafast Optical Excitation of a Persistent Surface-State Population in the Topological Insulator Bi<sub>2</sub>Se<sub>3</sub>. *Phys. Rev. Lett.* **2012**, *108* (11), 117403.
- (37) Wang, Y. H.; Hsieh, D.; Sie, E. J.; Steinberg, H.; Gardner, D. R.; Lee, Y. S.; Jarillo-Herrero, P.; Gedik, N. Measurement of Intrinsic Dirac Fermion Cooling on the Surface of the Topological Insulator Bi<sub>2</sub>Se<sub>3</sub> Using Time-Resolved and Angle-Resolved Photoemission Spectroscopy. *Phys. Rev. Lett.* **2012**, *109* (12), 127401.

- (38) Hamh, S. Y.; Park, S. H.; Jerng, S. K.; Jeon, J. H.; Chun, S. H.; Jeon, J. H.; Kahng, S. J.; Yu, K.; Choi, E. J.; Kim, S.; Choi, S. H.; Bansal, N.; Oh, S.; Park, J.; Kho, B.-W.; Kim, J. S.; Lee, J. S. Surface and interface states of Bi2Se3 thin films investigated by optical second-harmonic generation and terahertz emission. *Appl. Phys. Lett.* **2016**, *108* (5), 051609.
- (39) Hamh, S. Y.; Park, S. H.; Jerng, S. K.; Jeon, J. H.; Chun, S. H.; Lee, J. S. Helicity-dependent photocurrent in a Bi<sub>2</sub>Se<sub>3</sub> thin film probed by terahertz emission spectroscopy. *Phys. Rev. B: Condens. Matter Mater. Phys.* **2016**, DOI: 10.1103/PhysRevB.94.161405.
- (40) Braun, L.; Mussler, G.; Hruban, A.; Konczykowski, M.; Schumann, T.; Wolf, M.; Münzenberg, M.; Perfetti, L.; Kampfrath, T. Ultrafast photocurrents at the surface of the three-dimensional topological insulator Bi<sub>2</sub>Se<sub>3</sub>. *Nat. Commun.* **2016**, *7*, 13259. Supplementary Information: http://www.nature.com/articles/ncomms13259#supplementary-information.
- (41) Sim, S.; Brahlek, M.; Koirala, N.; Cha, S.; Oh, S.; Choi, H. Ultrafast terahertz dynamics of hot Dirac-electron surface scattering in the topological insulator Bi<sub>2</sub>Se<sub>3</sub>. *Phys. Rev. B: Condens. Matter Mater. Phys.* **2014**, 89 (16), 165137.
- (42) Qi, J.; Chen, X.; Yu, W.; Cadden-Zimansky, P.; Smirnov, D.; Tolk, N. H.; Miotkowski, I.; Cao, H.; Chen, Y. P.; Wu, Y.; Qiao, S.; Jiang, Z. Ultrafast carrier and phonon dynamics in Bi<sub>2</sub>Se<sub>3</sub> crystals. *Appl. Phys. Lett.* **2010**, *97* (18), 182102.
- (43) Luo, L.; Yang, X.; Liu, X.; Liu, Z.; Vaswani, C.; Cheng, D.; Mootz, M.; Zhao, X.; Yao, Y.; Wang, C. Z.; Ho, K. M.; Perakis, I. E.; Dobrowolska, M.; Furdyna, J. K.; Wang, J. Ultrafast manipulation of topologically enhanced surface transport driven by mid-infrared and terahertz pulses in Bi<sub>2</sub>Se<sub>3</sub>. *Nat. Commun.* **2019**, *10* (1), 607.
- (44) Ginley, T. P.; Law, S. Growth of Bi<sub>2</sub>Se<sub>3</sub> topological insulator films using a selenium cracker source. J. Vac. Sci. Technol., B: Nanotechnol. Microelectron.: Mater., Process., Meas., Phenom. 2016, 34 (2), No. 02L105.
- (45) Wang, Y.; Law, S. Optical properties of  $(Bi_{1-x}In_x)_2Se_3$  thin films. Opt. Mater. Express 2018, 8 (9), 2570–2578.
- (46) Tarakina, N. V.; Schreyeck, S.; Luysberg, M.; Grauer, S.; Schumacher, C.; Karczewski, G.; Brunner, K.; Gould, C.; Buhmann, H.; Dunin-Borkowski, R. E.; Molenkamp, L. W. Suppressing Twin Formation in Bi2Se3 Thin Films. *Adv. Mater. Interfaces* **2014**, *1* (5), 1400134.
- (47) Valdés Aguilar, R.; Stier, A. V.; Liu, W.; Bilbro, L. S.; George, D. K.; Bansal, N.; Wu, L.; Cerne, J.; Markelz, A. G.; Oh, S.; Armitage, N. P. Terahertz Response and Colossal Kerr Rotation from the Surface States of the Topological Insulator Bi<sub>2</sub>Se<sub>3</sub>. *Phys. Rev. Lett.* **2012**, *108* (8), No. 087403.
- (48) Smith, N. Classical generalization of the Drude formula for the optical conductivity. *Phys. Rev. B: Condens. Matter Mater. Phys.* **2001**, DOI: 10.1103/PhysRevB.64.155106.
- (49) Cocker, T. L.; Baillie, D.; Buruma, M.; Titova, L. V.; Sydora, R. D.; Marsiglio, F.; Hegmann, F. A. Microscopic origin of the Drude—Smith model. *Phys. Rev. B: Condens. Matter Mater. Phys.* **2017**, *96* (20), 205439.
- (50) Cocker, T. L.; Titova, L. V.; Fourmaux, S.; Bandulet, H. C.; Brassard, D.; Kieffer, J. C.; El Khakani, M. A.; Hegmann, F. A. Terahertz conductivity of the metal-insulator transition in a nanogranular VO2 film. *Appl. Phys. Lett.* **2010**, *97* (22), 221905.
- (51) Cocker, T. L.; Titova, L. V.; Fourmaux, S.; Holloway, G.; Bandulet, H. C.; Brassard, D.; Kieffer, J. C.; El Khakani, M. A.; Hegmann, F. A. Phase diagram of the ultrafast photoinduced insulator-metal transition in vanadium dioxide. *Phys. Rev. B: Condens. Matter Mater. Phys.* **2012**, DOI: 10.1103/PhysRevB.85.155120.
- (52) Titova, L. V.; Cocker, T. L.; Cooke, D. G.; Wang, X.; Meldrum, A.; Hegmann, F. A. Ultrafast percolative transport dynamics in silicon nanocrystal films. *Phys. Rev. B: Condens. Matter Mater. Phys.* **2011**, DOI: 10.1103/PhysRevB.83.085403.
- (53) Titova, L. V.; Cocker, T. L.; Xu, S.; Baribeau, J.-M.; Wu, X.; Lockwood, D. J.; Hegmann, F. A. Ultrafast carrier dynamics and the role of grain boundaries in polycrystalline silicon thin films grown by

- molecular beam epitaxy. Semicond. Sci. Technol. 2016, 31 (10), 105017.
- (54) Richter, C.; Schmuttenmaer, C. A. Exciton-like trap states limit electron mobility in TiO<sub>2</sub> nanotubes. *Nat. Nanotechnol.* **2010**, *5*, 769. Supplementary Information: https://www.nature.com/articles/nnano.2010.196#supplementary-information.
- (55) Turner, G. M.; Beard, M. C.; Schmuttenmaer, C. A. Carrier localization and cooling in dye-sensitized nanocrystalline titanium dioxide. *J. Phys. Chem. B* **2002**, *106* (45), 11716–11719.
- (56) Jensen, S. A.; Ulbricht, R.; Narita, A.; Feng, X.; Mullen, K.; Hertel, T.; Turchinovich, D.; Bonn, M. Ultrafast photoconductivity of graphene nanoribbons and carbon nanotubes. *Nano Lett.* **2013**, *13* (12), 5925–30.